Collective Hydrogen Bond Reorganization in Water Studied with Temperature-Dependent Ultrafast Infrared Spectroscopy

Field Code Changed
Field Code Changed
Field Code Changed

Collective Hydrogen Bond Reorganization in Water Studied with Temperature-Dependent Ultrafast Infrared Spectroscopy

Rebecca A. Nicodemus, S. A. Corcelli,# J. L. Skinner,+ and Andrei Tokmakoff**

*Department of Chemistry, Massachusetts Institute of Technology, Cambridge, MA 02139

[#]Department of Chemistry, University of Notre Dame, Notre Dame, IN 46556

[+]Department of Chemistry, University of Wisconsin, Madison, WI 53706

Abstract

We use temperature-dependent ultrafast infrared spectroscopy of dilute HOD in H_2O to study the picosecond reorganization of the hydrogen bond network of liquid water. Temperature-dependent two-dimensional infrared (2D IR), pump-probe, and linear absorption measurements are self-consistently analyzed with a response function formalism that includes the effects of spectral diffusion, population lifetime, reorientational motion, and non-equilibrium heating of the local environment upon vibrational relaxation. Over the range of 278 to 345 K, we find the time scales of spectral diffusion and reorientational relaxation decrease from approximately 2.4 to 0.7 ps and 4.6 to 1.2 ps, respectively, which corresponds to the barrier heights of 3.4 and 3.7 kcal/mol, respectively. We compare the temperature dependence of the time scales to a number of measures of structural relaxation and find similar effective activation barrier heights and slightly non-Arrhenius behavior, which suggests that the reaction coordinate for the hydrogen bond rearrangement in water is collective. Frequency and orientational correlation functions computed from molecular dynamics (MD) simulations over the same temperature range support our interpretations. Finally, we find the lifetime of the OD stretch is nearly the same from 278 K to room temperature and then increases as the temperature is increased to 345 K.

Keywords: Dynamics, Kinetics, Hydrogen-Bond Rearrangement, Infrared Spectroscopy, Arrhenius, Molecular Dynamics, Water

I. Introduction

Despite years of extensive study and continuous improvements in experimental and theoretical methods, the femtosecond-to-picosecond dynamics that describe changes to the hydrogen bonding structure of water continue to be difficult to describe. Being a dense medium, liquid intermolecular dynamics involve the collective motion of large numbers of molecules, for which translational and rotational degrees of freedom are strongly intertwined. This complexity is heightened in the case of the water due to its locally structured hydrogen bond network. The details of structural relaxation in water have been studied by molecular dynamics (MD) simulations beginning with the original work of Rahman and Stillinger.[1] Intermolecular motions and the interconversion between structures have been analyzed in a number of ways including through groups, chains, polyhedra, clathrate structures, inherent structures, and instantaneous normal modes.[2,3] No correlations between local structural variables, such as hydrogen bond participation, exist between configurational states separated by more than a few picoseconds.[4] Therefore, the dynamics of structural relaxation processes are not readily described in terms of structure on molecular length scales.

Recent experimental and theoretical studies of water have provided new perspectives on the local dynamics of hydrogen bonding, describing in detail how the hydrogen bond distances and angular motions change during the course of collective structural reorganizations.[5-7] With ultrafast infrared spectroscopy and MD simulations, Eaves et al. observed that water molecules in broken or strained hydrogen bond configurations return to a stable hydrogen bond within the fastest intermolecular motions suggesting that hydrogen bond switching is a concerted process.[5] Laage and Hynes performed MD

simulations and found the dominant mechanism of reorientation is through large amplitude angular jumps with a contribution from diffusive reorientation of the intermolecular OO framework.[6] In these studies, molecular motions that have been identified as important for reorganization include concerted hydrogen bond switching, large angle jumps, translation within the first and second solvation shells, and diffusive reorientation of a hydrogen bonded pair of water molecules.

It is important to recognize that local geometric variables are just different parameters that capture motion along a collective reaction coordinate. Different motions may be projected from the collective dynamics and certain coordinates may project more favorably than others. However, long time relaxation phenomena of internal variables should all decay in a correlated fashion.[8] Absolute time scales from different experiments are difficult to compare since the observables are sensitive to different relaxation processes, yet the temperature dependence should be identical if they all are sensitive to the same collective reaction coordinate.

In this paper we report on the temperature dependence of spectral diffusion and reorientation of the OD stretch of dilute HOD in H_2O to determine if the relaxation of these different measures of water structural change are correlated. In order to quantify the temperature-dependent time scales we self-consistently model the pump-probe anisotropy, vibrational relaxation, and spectral diffusion with a response function formalism that includes the bath H_2O stretch and combination band and the thermally shifted ground state (TSGS) of all three modes. We find a similar barrier height for both spectral diffusion and reorientation along with a number of other measurements that are sensitive to collective and single molecule relaxation of water. We also observe a similar

behavior for spectral diffusion and reorientation calculated with MD simulations with the SPC-FQ[9] model of water. Finally, the temperature dependence of the vibrational lifetime of the OD stretch suggests that the relaxation pathway may not be fully understood and more information may be gained with further theoretical and experimental studies.

II. Methods

A. Experimental

Temperature-dependent Fourier transform infrared (FTIR) absorption spectra of dilute HOD in H_2O were collected at 1 cm^{-1} resolution with a Nicolet 380 FTIR spectrometer from Thermo-Electron Corporation. The sample was contained between 1 mm thick CaF_2 windows with a path length of 6 μm set by a Teflon spacer for both linear and nonlinear measurements. The temperature of the home built brass sample cell was controlled with a water-cooled chiller, Neslab RTE-7.

Sub-100 fs infrared pulses were generated with a home-built system consisting of an amplified Ti:sapphire pulse (800 nm, 1 kHz, 1 W) pumping an optical parametric amplifier (OPA). A small portion of 800 nm (~1%) creates white light in a sapphire plate. After the white light seed and a portion of the 800 nm (~9%) pass through a 3 mm β-Barium Borate (BBO) crystal, the idler (2 μm) seeds a second pass through the BBO with the remaining 800 nm. Mid-infrared light is created by difference frequency generation of the signal (1.33 μm) and idler in a 0.5 mm $AgGaS_2$ crystal. The spectrum was centered at 2500 cm^{-1} with a FWHM of ~230 cm^{-1}. Although the infrared pulse was contained in a purged box there was still residual CO_2 creating a dip in the spectrum. The pulses were compressed to ~70 fs for the 2D measurements and ~80 fs for the pump-

probe (PP) measurements. Cross phase modulation (XPM) obscures spectral information within approximately two times the pulse width. Pulse delays were controlled with a pair of AR-coated ZnSe wedges mounted to stages that translate the wedge face perpendicular to the beam path. The ZnSe wedges are 6 cm in length and have a 1.2° wedge.

We measured temperature-dependent two-dimensional infrared (2D IR) surfaces in the parallel polarization geometry to characterize spectral diffusion. We use KBr beam splitters to split the mid-infrared pulse into three parts to acquire surfaces in the pump-probe geometry in which a collinear pulse pair creates a vibrational excitation, and the third pulse acts as the probe and local oscillator.[10] The measured signal is the real part of the rephasing plus non-rephasing pathways.[11] The τ_1-axis was created by step-scanning the non-chopped pump beam in 2 fs steps to 600 fs. Scanning the non-chopped pump beam removes the contribution to the total signal of the τ_1-dependent PP between the probe and one of the pump beams. The PP between the probe and the other pump beam is independent of τ_1 and is, therefore, removed by numerical Fourier transform to create the excitation, or ω_1, dimension. The probe beam is spectrally dispersed after the sample with a 75-grooves/mm grating onto a 64-channel liquid nitrogen cooled MCT array. The ~6 cm^{-1} resolution in ω_3 gives a detection axis with 400 cm^{-1} bandwidth. In addition to the acquisition of the 2D signal, the interferometric autocorrelation and interference fringes for stage calibration are simultaneously measured from the replica of the collinear pump pair from the backside of the recombining beam splitter.[10] A small reflection is directed into a room temperature MCT to measure the interferometric autocorrelation that constrains the relative pulse timing to the step size. The remainder is passed through a monochromater set to 2500 cm^{-1} with a resolution of 1 cm^{-1}, and the interference is

collected with a single channel MCT detector and Fourier transformed to determine the correction to the τ_1-axis.[10]

We used polarization-selective transient absorption to study temperature-dependent reorientational dynamics and vibrational relaxation. In the pump-probe geometry a pump-probe can be measured simply by blocking the non-chopped pump beam. A MgF_2 $\lambda/2$-waveplate (Alphalas) is placed in the pump path to rotate the polarization 45° relative to the probe. The polarization of the pump and probe were selected with ZnSe wire-grid polarizers (Molectron). There are two polarizers after the sample. The analyzing polarizer is rotated between parallel and perpendicular relative to the pump. The second polarizer is set parallel to the probe such that the polarization-sensitive grating sees the same polarization for zzzz and zzyy measurements. The pump-probe measurements were acquired by fast scanning the delay time and averaging the scans. The isotropic signal, which is free of rotations and therefore measures vibrational relaxation, is constructed from the zzzz and zzyy measurements as: $S_{iso}(\tau_2) = \left(S_{zzzz}(\tau_2) + 2S_{zzyy}(\tau_2)\right)/3$. The anisotropy, which measures reorientational dynamics, is constructed as: $C_R(\tau_2) = \left(S_{zzzz}(\tau_2) - S_{zzyy}(\tau_2)\right)/\left(S_{zzzz}(\tau_2) + 2S_{zzyy}(\tau_2)\right)$.

B. Molecular Dynamics Simulations

The MD simulations of neat H_2O using the electronically polarizable SPC-FQ[9] model have been described previously.[12] Here we will summarize the most salient details. In the SPC-FQ model the geometry of the individual water molecules is held rigid with an OH bond length of 1 Å and an HOH angle of 109.47°. SPC-FQ models electronic

polarizability by allowing its three atomic centered point charges to fluctuate based on the instantaneous environment of the water molecule. In principle, the charges could be calculated self-consistently at each MD time step, but in practice the charges are regarded as dynamical variables in an extended Lagrangian and propagated in time.[9] This elegant approach results in a substantial computational savings. There are three reasons why the SPC-FQ model was chosen for this work on the temperature-dependent ultrafast IR spectroscopy of HOD/H_2O: (1) Previous studies at room temperature have shown that the SPC-FQ model exhibits rotational dynamics that are in better agreement with experiment than other commonly employed non polarizable water models (e.g. TIP4P[13] and SPC/E[14]).[9] (2) At room temperature the longest time scale for the decay of the frequency fluctuation time correlation function is also in better agreement with experiment than TIP4P and SPC/E.[15] (3) The IR absorption and Raman scattering spectra computed for SPC-FQ are in excellent agreement with experiment from 10 – 90 °C.[12]

We calculated trajectories of 128 SPC-FQ H_2O molecules at five temperatures in cubic boxes whose sizes were chosen to mimic the experimental number density at 283, 303, 323, 343, and 363 K. The 1 ns trajectories were collected in the NVE ensemble with a 0.5 fs time step, where the charge degrees of freedom were maintained at 5 K by rescaling the charge velocities every 1000 steps. A running average of the temperature was monitored to ensure that it did not deviate outside of ±1.5 K of the target temperature. Other details regarding the MD simulations are contained in Reference[12].

Two quantities were computed from the trajectories: the OH bond orientational correlation function, $C_R(t) = \langle P_2[\hat{u}_{OH}(0) \cdot \hat{u}_{OH}(t)] \rangle$, where P_2 is the 2nd Legendre polynomial and $\hat{u}_{OH}(t)$ is a unit vector that points along an OH bond, and the normalized

electric field fluctuation time correlation function, $C_E(t) = \langle \delta E_{OD}(0) \delta E_{OD}(t) \rangle / \langle (\delta E_{OD})^2 \rangle$, where $E_{OD}(t)$ is the magnitude of the electric field, due to the surrounding water molecules, along an OH bond of interest and $\delta E_{OD}(t) = E_{OD}(t) - \langle E_{OD} \rangle$ represents the fluctuation of $E_{OD}(t)$ from its equilibrium value, $\langle E_{OD} \rangle$. $C_R(t)$ was computed for the 256 independent OH bonds in the simulations. Although the simulations were of neat H_2O, for the purposes of computing $C_E(t)$ each of the bonds in the simulation were assumed to be the OD stretch of interest, which assumes that the dynamics of a single HOD molecule in water are similar to that of an H_2O molecule. The electric fields along each OH bond were then computed using the instantaneous charges on each of the other 127 water molecules in the simulation, where the effects of long ranged electrostatics were incorporated using an approximation to the Ewald sum.[16]

The rationale for computing the normalized electric field fluctuating correlation function is that, within certain approximations, $C_E(t)$ is equal to the normalized frequency fluctuation correlation function, $C_\omega(t)$, which can be extracted from the ultrafast 2D IR measurements on HOD in H_2O. The key assumption needed to connect $C_E(t)$ with $C_\omega(t)$ is that the instantaneous OD vibrational frequency of interest can be linearly related to the electric field along the bond, $\omega_{OD} = a + bE_{OD}$. Previous density functional theory calculations on 100 HOD·$(H_2O)_n$ clusters containing between 4 and 9 water molecules extracted from a room temperature MD simulation have empirically established a linear relationship (a = 2745.8 cm^{-1} and b = 4870.3 cm^{-1}/au) between the OD stretch frequency of HOD with the electric field due to the surrounding solvent along its bond. It is important to note, as a caveat, that more recent work on more and larger

clusters, albeit for different water models, have found that quadratic relationships between the electric field and vibrational frequency are more appropriate.[17, Auer, 2008 #2979] Nevertheless, for discerning trends in the long time decay of the frequency fluctuation correlation function as a function of temperature, invoking the approximately linear relationship available from the previous literature is reasonable.

III. Results

Temperature-dependent linear absorption of the OD stretch of HOD in H_2O at the five temperatures in this study (278, 286, 295, 323, and 345 K) with the background H_2O subtracted are shown in Figure 1a and without subtraction in Figure 1b. The condensed phase spectra red shifts by ~215 cm^{-1} from the gas phase (2723.68 cm^{-1})[18] due to hydrogen bonding. The ~160 cm^{-1} full-width half maximum (FWHM) primarily reflects a distribution of hydrogen bond strengths (see the supporting information).[19] From 278 to 345 K the peak blue shifts from 2499 to 2534 cm^{-1} (0.53 cm^{-1}/K), indicating an increase in hydrogen bond fluctuations, and the FWHM broadens from 159 to 180 cm^{-1}. However, the total area decreases with increasing temperature due to the non-Condon effect.[20,21] In the same temperature range the HOD bend, which can be seen in Figure 1b, narrows and red shifts from 1460 to 1450 cm^{-1}. The model calculations, which will be described below, include the combination band ($\nu_L + \nu_B$) and stretch of the H_2O bath. From 278 to 345 K the H_2O stretch red shifts from 3389 to 3433 cm^{-1} (0.66 cm^{-1}/K) and the combination band blue shifts from 2134 to 2075 cm^{-1} (quadratic dependence with temperature).

Isotropic transient absorption at each of the five temperatures is shown in Figure 2a. The isotropic PP is calculated from the zzzz and zzyy transient absorption measurements by the relationship given above. The dispersed PP is integrated over 75% of the maximum in frequency (of a slice taken at τ_2 = 200 fs to avoid XPM) to take into account the change in center frequency with temperature. Thermalization of the low frequency modes occurs upon vibrational relaxation of the OD stretch. This causes a blue shift in the frequency of the stretch that prevents refilling of the ground state bleach. At long waiting times the thermally shifted ground state (TSGS) appears as a difference spectrum between linear spectra separated by ~1 K.[22] The TSGS has been included in a fit model by Rezus and Bakker[23] that also includes relaxation through an intermediate state. The fit model does not consider effects from the vibrational Stokes shift. The experimental vibrational lifetimes found by applying the fit model starting at τ_2 = 400 fs for each of the five temperatures are shown in Figure 3. We find a similar lifetime for the three lowest temperatures (~1.45 ps) and an increase in lifetime above room temperature to 2.0 ps at the highest temperature (345 K). The intermediate state lifetime increases slightly with temperature, changing from 450 fs to 590 fs from 278 to 345 K (not shown). We found that fitting the integrated isotropic transient absorptions assuming that the TSGS grows in at the same rate as the decay of the excited state resulted in fits of similar quality within our experimental time window (~4 ps).

Normalized temperature-dependent pump-probe anisotropies are shown in Figure 2b. Before calculating the pump-probe anisotropy, the bi-exponential growth of the TSGS, determined by fitting the isotropic PP, is subtracted from the zzzz and zzyy transient absorption measurements. This approach assumes the TSGS does not depend

on the polarization, which has been shown to be a reasonable assumption for the OD stretch.[24] The dispersed anisotropies are integrated over a frequency range set by the maximum in frequency of a slice in the isotropic signal at τ_2 = 200 fs. Although XPM obscures spectral information within the first ~150 fs, we fit the anisotropies with a bi-exponential beginning at 200 fs since a bi-exponential decay has previously been observed with shorter pulses for the OH stretch of HOD in D_2O.[25] The inertial decay is set to 50 fs for all temperatures, the inertial time scale measured for the OH stretch of HOD in D_2O at room temperature,[25] and the initial value is set to 0.4. We do not observe a clear trend between the inertial amplitude and temperature in the bi-exponential fits. MD simulations predict the inertial amplitude will increase with increasing temperature but experiments have reported that there is a change in frequency dependence of the inertial component with temperature, which complicates a straightforward relationship.[26,27] The long time decay of the anisotropy, shown in Figure 3, becomes faster with increasing temperature. We found very similar values for the long-time decay when fitting a single exponential beginning at 200 fs without constraining the initial value.

2D IR surfaces at each of the five temperatures at three different waiting times are shown in Figure 4. 2D surfaces at five waiting times and two temperatures have previously been published.[28] Since multiple vibrational levels are accessible within the bandwidth of our pulse, the 2D surface displays a positive peak from ground state bleach (ν=1←0) and an anharmonically shifted negative peak from excited state absorption (ν=2←1). At early waiting times ($\tau_2 < \tau_C$, where τ_C represents the correlation time), the peaks are diagonally elongated indicating frequency correlation between the first and

third time periods. In the top row of Figure 4 we show 2D surfaces at τ_2 = 160 fs for each of the five temperatures. Notice at 278 K the pear shape of the positive peak where the anti-diagonal line width is narrow on the red side and relatively broad on the blue side (where red and blue refer to low and high frequencies relative to band center, respectively). The asymmetry across the line width forms the basis of a previous publication in which we analyze the waiting time dependence of the line shape for the OH stretch of dilute HOD in D_2O and find that strained or broken hydrogen bonds exist only fleetingly.[5,29] Note that as the temperature is increased, but as the waiting time is kept constant, the asymmetry across the line shape decreases and the anti-diagonal line width becomes generally broader. We also plot the phase representation of the surfaces. We detail how we extract the complex surface from the measured real surface in the supporting information. At early waiting times the phase lines are tilted toward the diagonal. At τ_2 = 400 fs (second row of Figure 4) the frequencies initially excited have more time to diffuse through the line shape. As a result the peaks are more symmetric, or appear more homogeneous, and the phase lines have tilted toward ω_1 at all temperatures. Notice, however, at low temperature the line shape is more inhomogeneous relative to high temperature. At long waiting times ($\tau_2 > \tau_C$), sufficient spectral diffusion occurs during the waiting time such that peaks appear round due to loss of correlation. Also, an additional negative feature appears above the diagonal upon sufficient vibrational relaxation due to the TSGS. In the third row of Figure 4 we show the temperature-dependent 2D surfaces at 3.2 ps. Note the surfaces are generally round and there is additional negative feature above the diagonal, particularly visible for the three lowest temperatures, that acts to narrow the positive amplitude along ω_3. Finally, note that there

appears to be a residual inhomogeneity, especially apparent at higher temperatures in the phase representation, on the red side of the spectrum.

We used a number of metrics that have previously been defined[30] to characterize the waiting time dependence of spectral diffusion including the dynamic line width,[31] slope of the node,[22,32] and the center line slope.[33] After retrieving the complex correlation spectrum and the rephasing and non-rephasing surfaces on the basis of the Kramers-Kronig assumption (see the supporting information) we also considered the normalized difference of the amplitude of the rephasing to non-rephasing surfaces,[30] the slope of the imaginary node, and the phase line slope (PLS).[22,28] All metrics show a similar trend with waiting time and temperature. In Figure 2c we show the phase line slope, $\tan(\varphi)$, over frequencies marked with the box in the phase representation in Figure 4 ($\omega_1 = \omega_3 = 2470$ to 2530 cm^{-1}) for each temperature. In our previous publication we set the bounds of the box to 90% of the maximum in ω_1 and ω_3 for each surface.[28] Both treatments show a very similar behavior. The phase line slope decreases with increasing temperature. However, there is an offset that appears larger with increasing temperature.

IV. Spectroscopic Model

In order to quantify the temperature-dependence of spectral diffusion, reorientational dynamics, and vibrational relaxation, we employ a widely used nonlinear response function formalism to self-consistently model the FTIR, PP and 2D IR measurements.[34] The model is similar to one we used to study the OH stretch of HOD in D_2O.[35] The response function, S, describes the vibrational dynamics of OD dephasing (S_ω), vibrational population relaxation (S_{pop}), and reorientation (Y) as separable

contributions to the vibronic response function, in addition to non-equilibrium heating effects that arise from vibrational relaxation of the OD stretch (S_{TSGS}):

$$S = Y\left(S_{\omega}S_{pop,\omega} + S_{TSGS}S_{pop,TSGS}\right) \tag{1}$$

Dephasing is treated as fluctuations of the ν = 0, 1, and 2 system eigenstates that result from coupling to a harmonic bath characterized by a bath time-correlation function, $C_{\omega}(t)$. The remaining components are treated as phenomenological rate processes.

This model makes several approximations that assume the various dynamics can be treated as homogeneous processes. We use the Condon and second-order cumulant approximations,[34,36] which state that the transition dipole moment is independent of bath, and that the frequency fluctuations are purely Gaussian. Both approximations have been shown to be invalid for water on time scales short compared to spectral diffusion.[12,20,21,29,37] Rotation and vibrational relaxation are treated as Markovian processes that are independent of vibrational dephasing, although evidence indicates that this is a poor assumption for the same short time scales. We proceed with this analysis since the emphasis of this study is on relaxation kinetics on time-scales longer than the correlation time for spectral diffusion. On these long time-scales structural reorganization of the hydrogen bond network has effectively scrambled correlations among the different relaxation processes.

The timescale on which the assumptions become valid can be deduced from an analysis of heterogeneity within the 2D IR line shape. In Figure 5a we show the waiting time-dependence of the first moment of the positive signal distribution for slices in ω_1 on the red and blue side of the line shape at 295 K.[29] The decrease in the first moment on

both sides of the line width at longer waiting times is due to the growth of the TSGS. For $\tau_2 \leq 200$ fs, there is a significant difference between first moment on the red and blue side, with a fast decrease on the blue side and a slight recurrence at ~120 fs on the red side. A recurrence, or beat, has been observed in previous PS and 2D IR measurements of the OH stretch[35] and MD simulations of the OH and OD stretch (for certain water models).[38] After approximately 500 fs the dynamics become more similar across the line width. At 278 K (Figure 5b), similar observations are made, but the difference across the line width is somewhat larger. Also, the recurrence on the red side of the line width is more pronounced at the lower temperature. These observations indicate that our model properly handles the measurement of relaxation time-scales for waiting times longer than the OD frequency correlation time.

A. Vibrational Dephasing

To model the vibrational dephasing response function S_{ω}, we include rephasing (–) and non-rephasing (+) pathways that contribute to third-order nonlinear experiments for pulses separated in time. Within the Condon approximation, and combining the dephasing and vibrational population relaxation, $S_{\omega}S_{pop}$, the rephasing (S_{-}) and nonrephasing (S_{+}) response functions are

$$S_{-}(\tau_3,\tau_2,\tau_1) = \left|\mu_{10}\right|^2 \exp[-\frac{\tau_2}{T_1}]\exp[i\left\langle\omega_{10}\right\rangle\tau_1 - \frac{\tau_1}{2T_1}]$$
$$\times\{\left|\mu_{10}\right|^2 \exp[-i\left\langle\omega_{10}\right\rangle\tau_3 - \frac{\tau_3}{2T_1}][F^{(3)}_{0101}(\tau_3,\tau_2,\tau_1) + F^{(4)}_{0101}(\tau_3,\tau_2,\tau_1)] \quad (2a)$$
$$-\left|\mu_{21}\right|^2 \exp[-\left\langle\omega_{21}\right\rangle\tau_3 - \frac{3\tau_3}{2T_1}][F^{(2)}_{0121}(\tau_3,\tau_2,\tau_1)]^*\},$$

$$S_{+}(\tau_3,\tau_2,\tau_1) = \left|\mu_{10}\right|^2 \exp[-\frac{\tau_2}{T_1}]\exp[-i\left\langle\omega_{10}\right\rangle\tau_1 - \frac{\tau_1}{2T_1}]$$
$$\times\{\left|\mu_{10}\right|^2 \exp[-i\left\langle\omega_{10}\right\rangle\tau_3 - \frac{\tau_3}{2T_1}][F^{(1)}_{0101}(\tau_3,\tau_2,\tau_1) + F^{(2)}_{0101}(\tau_3,\tau_2,\tau_1)] \quad (2b)$$
$$-\left|\mu_{21}\right|^2 \exp[-\left\langle\omega_{21}\right\rangle\tau_3 - \frac{3\tau_3}{2T_1}][F^{(4)}_{0121}(\tau_3,\tau_2,\tau_1)]^*\}.$$

In these expressions ω_{10}, ω_{21} and μ_{10}, μ_{21} denote the transition frequency and transition dipole of the ν=1←0 and ν=2←1 transitions, respectively. The room temperature anharmonicity is fixed at $\omega_{10} - \omega_{21}$ = 162 cm^{-1} for the OD stretch[31] and is taken to be independent of temperature. We assume harmonic scaling of the transition dipole, therefore $\mu_{21} = \sqrt{2}\mu_{10}$. F_{abcd} are the dephasing functions, in which the indices refer to the vibrational 0, 1 and 2 states. The dephasing functions, which depend on the two-point frequency correlation function, are given in the supporting information. T_1 is the vibrational lifetime, which is determined by fitting the isotropic transient absorption. We include population relaxation during the coherence periods with the timescale determined by: Γ_{ab} = ½(Γ_{aa} + Γ_{bb}), where T_1=1/Γ_{11}. We assume the population relaxation scales with quantum number, Γ_{aa} = aΓ_{11}, therefore T_1 is the only necessary input.

Motivated by a number of observations, we use a complex frequency correlation function in the present work.[34] First, librational motion plays an important role in the

short time dynamics, and it is unclear if the high-temperature limit applies to librational frequencies. Also, harmonic bath models make explicit predictions about the temperature dependence of spectroscopic observables; for instance, the absorption line width is linear in T in the high temperature limit. Also, the Stokes shift, which accounts for the response of the bath to OD excitation, has been predicted to be small but a relevant contribution to the spectroscopy. A complex correlation function can be used to properly account for these effects. Computational modeling of HOD in H_2O indicated that a classical correlation function is satisfactory for linear measurements, but quantum effects may become important for nonlinear measurements, especially for strongly inhomogeneously broadened systems.[39] Overall, the analysis with a complex correlation function did not differ greatly from a real correlation function, but the modeling does identify interesting aspects that are discussed below and in the supporting information.

Similar to prior studies of HOD in H_2O by Fayer and co-workers,[31] a tri-exponential was chosen as the functional form of the frequency correlation function:[34]

$$C_{\omega}(t) = \sum_{j=1}^{3} A_j \left[\frac{1}{\tau_{C,j}} \coth\left(\frac{\hbar}{2k_B T \tau_{C,j}} \right) - i \frac{1}{\tau_{C,j}} \right] \exp\left(\frac{-t}{\tau_{C,j}} \right). \quad (3)$$

In this equation $\tau_{C,j}$ is the correlation time for the j^{th} exponential relaxation component and A_j is its amplitude. For this model, the reorganization energy is $\lambda = \sum_j A_j$, and 2λ is the Stokes shift. For a correlation function comprised of exponentials the expression for the line shape function becomes:[34]

$$g(t) = \sum_j A_j \left[\tau_{C,j} \coth\left(\frac{\hbar}{2k_B T \tau_{C,j}} \right) - i\tau_{C,j} \right] \left[\exp\left(\frac{-t}{\tau_{C,j}} \right) + \frac{t}{\tau_{C,j}} - 1 \right] \quad (4)$$

Based on the simulations below we fixed the inertial decay time scale at $\tau_{C,1}$ = 50 fs for all five temperatures, although we found it necessary to vary the amplitude. To add constraints, we initially attempted to keep the intermediate timescale constant at $\tau_{C,2}$ = 400 fs, the intermediate timescale found by Fayer and co-workers,[31] but we found the fit of the two highest temperatures, 323 and 345 K, unsatisfactory. At these temperatures the intermediate timescale was set to 200 fs. Therefore, only three parameters of the frequency correlation function are independent: the timescale of the long-time decay, $\tau_{C,3,}$ and the amplitudes of the inertial and intermediate-time decays. A recurrence was not included in the correlation function since it is a relatively minor effect and we are primarily interested in the long-time behavior. In addition to the OD stretch of HOD, we also use this formalism to treat the weak background absorption from the H_2O stretch and libration-bend combination band.

B. Rotational Response

For the case that vibrational and orientational response functions are separable and reorientational motion is treated as a Markovian process, the nonlinear orientational correlation functions can be written in term of $C_{R,n}(t) = \langle P_n[\hat{\mu}(t)\cdot\hat{\mu}(0)]\rangle$, where P_n is the n^{th} order Legendre polynomial and $\hat{\mu}$ is the transition dipole unit vector.[40] The orientational responses are then expressed as:

$$Y_{zzzz}(\tau_3,\tau_2,\tau_1) = \frac{1}{9}C_{R,1}(\tau_1)\left[1+\frac{4}{5}C_{R,2}(\tau_2)\right]C_{R,1}(\tau_3), \quad (5)$$

$$Y_{zzyy}(\tau_3,\tau_2,\tau_1) = \frac{1}{9}C_{R,1}(\tau_1)\left[1-\frac{2}{5}C_{R,2}(\tau_2)\right]C_{R,1}(\tau_3). \quad (5)$$

For pump-probe measurements, the isotropic response $Y_{iso} = (Y_{zzzz} + 2Y_{zzyy})/3$ is observed to be independent of orientational dynamics during τ_2, whereas the anisotropy is proportional to the second order orientational correlation function: $C_R(\tau_2) = (2/5)C_{R,2}(\tau_2)$. Guided by observations from the MD simulations below and previous experimental results,[25] we model the anisotropy and second rank rotational correlation function as:

$$C_{R,2}(t,T) = \left(1 - A_R(T)\right)\exp\left(\frac{-t}{\tau_{inertial}}\right) + A_R(T)\exp\left(\frac{-t}{\tau_R(T)}\right). \quad (6)$$

An inertial reorientational response with a time-scale of $\tau_{inertial}$ = 50 fs is taken to be independent of temperature, but the amplitude A_R and reorientational correlation time τ_R are allowed to vary. For the purpose of describing 2D IR experiments, we include orientational relaxation during τ_1 and τ_3, which requires a first rank orientational correlation function, $C_{R,1}$. We relate $C_{R,1}$ and $C_{R,2}$ by scaling their orientational correlation times, but leave the inertial time scale unchanged. Based on recent MD simulations of water,[41] we use a scaling of $\tau_{R,1}/\tau_{R,2} = 2.3$, although the results are found to be indistinguishable within the model from the value of 3.0 predicted for small-angle diffusive reorientation. The linear spectrum, 2D IR and pump-probes are sensitive to the scaling; the pump-probe anisotropy, however, is not sensitive to the scaling within the model.

C. Thermal Effects

The model includes a third order response from the TSGS mentioned above for all three modes. The response can be written as:

$$S_{\pm}^{TSGS}(\tau_3,\tau_2,\tau_1) = A^{TSGS}\left|\mu_{10}\right|^4 N^{TSGS}(\tau_2)\exp\left(\mp i\left\langle\omega_{10}\right\rangle\tau_1 - i\left\langle\omega_{10}\right\rangle\tau_3\right) \times\exp\left(-g_{11}^{*}(\tau_1) - g_{11}(\tau_3)\right)\left[1-\left|\Delta\mu_{10}\right|^2\exp\left(-i\Delta\omega\tau_3\right)\right]. \quad (7)$$

In this equation $\Delta\mu_{10}$ denotes the decrease in transition dipole strength, $\Delta\mu_{10} = (\mu_{10} - \mu_{10}^{TSGS})/\mu_{10}$, and $\Delta\omega$ the blue-shift in frequency, $\Delta\omega = \omega_{10}^{TSGS} - \omega_{10}$, induced upon vibrational relaxation. This formalism assumes an uncorrelated TSGS,[35,42] in which frequency memory is lost upon vibrational relaxation. Temperature-dependent linear absorption spectra show that the frequency of the OD stretch changes linearly with temperature. Therefore, for all temperatures, $\Delta\omega$ is set to the frequency change for 1 K increase in temperature, 0.53 cm^{-1}. A^{TSGS}, the intensity of the thermally induced response, and $\Delta\mu_{10}$ are determined by fitting both the integrated isotropic PP at $\tau_2 > 1.5$ ps and the 2D surface at $\tau_2 = 4$ ps projected along ω_3.

$N^{TSGS}(\tau_2)$ represents the growth of the thermal response with waiting time determined by fitting the integrated isotropic PP measurements. The integrated isotropic PP is fit with the model developed by Bakker:[23]

$$N^{TSGS}(\tau_2) = 1 + \frac{1}{T_1 - T^*}\left[T^*\exp\left(-\tau_2/T^*\right) - T_1\exp\left(-\tau_2/T_1\right)\right] \quad (8)$$

In this equation T^* represents the lifetime of an intermediate state, which has been suggested to be the fundamental of the HOD bend.[43] Yeremenko and co-workers found an important contribution arising from the solvent D_2O in experiments on the OH stretch of HOD in D_2O.[44] However, this effect is small for absorptive 2D IR and PP

measurements, and is more important for measurements sensitive to dispersive changes, such as photon echo and transient grating.[45] Thermally induced shifts are also included for the background H_2O stretch and combination band, although the effect is rather small in the region of the OD stretch (see the supporting information).

D. Modeling Results

To apply the model to the OD stretch of HOD in H_2O we first fit the experimental integrated isotropic PP and PP anisotropy at each temperature to determine T_1, $N^{TSGS}(\tau_2)$, and $C_R(t)$. We make an initial guess for $C_\omega(t)$ and solve for λ by fitting the FWHM of the linear absorption measurement.[35] The isotropic PP and 2D IR surfaces are calculated and compared to experiment to determine A^{TSGS} and $\Delta\mu_{10}$. The complex surface is determined from the calculated 2D surfaces with the same method used for experimental 2D surfaces. The parameters for the frequency correlation function are adjusted at each temperature to best fit the experimental phase line slope over the same frequency range as the experiment. We allow for an arbitrary offset to the phase line slope generated from the model when comparing to the experimental phase line slope. Although we are interested in the long time behavior we fit the entire waiting time range to obtain the most reliable information. A self-consistent fitting of all the data provides enough constraints to quantitatively extract the longest correlation times, lifetimes, and reorganization energy at any temperature.

The reorganization energy, λ, is found by fitting the FWHM of the linear spectrum. The linear spectra calculated with the model are shown as solid lines in Figure 1. Since we are using the cumulant approximation the peaks are Gaussian. The reorganization

energy, λ, and the complex initial value of the frequency correlation function, $C_\omega(0)$, are given in Table 1. Since the frequency correlation function is complex, the calculated peak frequency, which is compared to the experimental value, is red-shifted from the input ω_{10} and we find that at a given temperature the magnitude of the red-shift was most sensitive to the amplitude of the inertial decay (an increased amplitude resulted in an increased red-shift). Experimental and input frequencies for the OD stretch are given in Table 1 along with the amplitudes and timescales of the temperature-dependent frequency correlation functions. The temperature-dependent long time decay is also shown in Figure 3. The amplitude of the inertial decay increases from 41% to 71% from 278 to 345 K. The amplitude of the intermediate and long-time decays both decrease with increasing temperature. The long-time decay decreases with increasing temperature, which is in agreement with our previous study.[28] The experimental phase line slopes and best fits with the model, including the offset, are shown as solid lines in Figure 2c.

2D IR spectra generated from the model with the best-fit frequency correlation functions are shown in Figure 6. The 2D surface is a 2D dimensional Fourier transform of $Y\left(S_\omega S_{pop,\omega} + S_{TSGS} S_{pop,TSGS}\right)$. The apparent asymmetry is in small part due to including the H_2O combination band and stretch but mainly due to windowing by the experimental pulse spectrum after the 2D surface is calculated. The 2D surfaces from the model are successful in capturing the average dynamics with waiting time and temperature. The model 2D IR surfaces agree with the experimental surfaces best at lower temperatures. As the temperature is increased the residual inhomogeneity on the red side of the line shape, which is not captured with the model, becomes more important.

After determination of the best-fit frequency correlation function the dispersed isotropic pump-probe is calculated using the isotropic orientational response function. The integrated isotropic signal from the model is compared to the experimental traces in Figure 2a. In order to compare the model and experimental anisotropy the third order response, without including the TSGS response, is calculated with the zzzz and zzyy orientational response functions. The comparison is shown in Figure 2b.

We explicitly include the background absorption of the combination band and stretch of the bath H_2O in our model to explore the origin of the long time offset observed in the phase line slope.[46,47] The H_2O combination band absorbs in the OD stretch region and there is a relatively small amount of absorption from the H_2O stretch. However, linear absorption and heterodyned third order measurements scale with the transition dipole to the second and fourth power, respectively. The molar absorptivity of the H_2O combination band and stretch are ~3.5 and ~100 M^{-1} cm^{-1} at the peak, respectively.[47] Given the sensitivity of the transition dipole on environment, with an increasing transition dipole with hydrogen bonding, it is not unreasonable for the H_2O stretch to contribute to the third order signal in the region of the OD stretch. We find, however, that including the bath H_2O was not important for the extracted dynamics from the model (see supporting information). Since H_2O was explicitly included in the model, all of the parameters discussed for the OD stretch had to be defined for the H_2O combination band and stretch. Parameters are given in the table and discussed in the supporting information.

V. Discussion

Over the past decade, the combination of ultrafast infrared spectroscopy and MD simulations of isotopically dilute water have developed an increasingly detailed molecular picture of the structural dynamics of water on the femtosecond to picosecond time scale. Since the frequency at which water absorbs is sensitive to its local environment, monitoring frequency evolution provides a picture of the evolving structure. On the picosecond time scale, theoretical work has shown that a number of relaxation mechanisms, including density and polarization fluctuations on length scales longer than the molecular diameter, occur on the same time scale as spectral diffusion suggesting that the picosecond time scale can not be assigned to local molecular motions but rather to collective rearrangements.[8,48] Although absolute time scales cannot be compared between experiments that are sensitive to different relaxation phenomena, if the structural evolution is collective the temperature dependence of these measurements will be correlated.

The inertial decay of the pump-probe anisotropy has been attributed to librations, or hindered rotations, of the OX (where X = H or D) transition dipole, and long time decay to collective reorientation.[25] The observed temperature-dependence of the long time relaxation agrees with previous studies using methods related to (with proper assumptions) the first Legendre polynomial: dielectric relaxation[49] and THz time domain spectroscopy;[50] and the second Legendre polynomial: NMR[51,52] and OKE.[53] Tielrooij and Bakker measured the temperature dependence of the reorientation time of the OD stretch of HOD in H_2O with ultrafast infrared spectroscopy and found it decreased from 4.8 to 0.97 ps from 274 to 343 K,[43] which is in reasonable agreement with our study. Assuming the long time decay follows Arrhenius behavior, $1/\tau_C = A\exp\left[-E_a/RT\right]$, we find a

barrier height of 3.7 kcal/mol compared to 4.1 kcal/mol found by Petersen and Bakker.[54] The Arrhenius plot in Figure 7 shows that the trend is nearly linear with a slight quadratic dependence.

Previous measurements of the spectral diffusion of isotopically dilute water have assigned the long-time decay to collective reorganization of the liquid structure.[8,35] Using the long-time decay from the temperature-dependent frequency correlation functions determined with the model (2.4 ps for 278 K to 0.7 ps for 345 K) and assuming Arrhenius behavior we find a barrier height of 3.4 kcal/mol. As can be seen in Figure 7 the trend is linear, with a slight quadratic dependence in an opposite manner as the reorientation. We also determined the barrier height for the integrated real part of the correlation functions and found 2.9 kcal/mol with a trend that is quite linear. Finally, in a previous publication we characterized the temperature-dependent spectral diffusion by fitting the phase slope decay with a number of functional forms and determining the correlation time either from the decay directly, integrating the normalized function, or from the 1/*e* period and found a barrier height of 3.4 ± 0.5 kcal/mol and a trend more similar to the reorientation.[28] The differences in barrier height and trend should be taken as the uncertainty in our determination of the picosecond spectral diffusion time scale.

As described in Section II.B, we calculated temperature-dependent frequency and OD intramolecular bond orientational correlation functions with MD simulations using the SPC-FQ[9] model for water. The polarizable SPC-FQ model was previously shown to provide a more accurate description than non-polarizable models (SPC/E and TIP4P) for the time scales of spectral diffusion and reorientational motion at room temperature compared to experiment.[15] Moreover, we previously examined the linear absorption

spectroscopy of the SPC-FQ water model in the range from 283 to 363 K and found excellent agreement with experiment. The results for the frequency time correlation functions, $C_{\omega}(t)$, and OD bond orientation correlation functions, $C_{R,2}(t)$ for five temperatures in the range from 283 to 363 K are shown in Figure 8a and 8b. The functions show the same trend as observed in the experiment: the long time decay is faster with increasing temperature. Also, we find that the inertial dynamics are roughly independent of temperature, although the amplitude does increase with temperature for the orientational correlation functions. We fit the picosecond decay with single exponentials and the time constants are shown in an Arrhenius plot in Figure 8c. The behavior is clearly nonlinear, which is similar, although more pronounced, than the experimental orientational relaxation and other observables (see Figure 7). Interestingly, the temperature-dependent trends for the two relaxation processes are similar within a scaling factor. Using temperature-dependent experimental NMR measurements of specific molecule-fixed unit vectors and MD simulations, Ropp et al. showed that rotational motion in water is anisotropic.[55] We have also determined the reorientational time scales from the picosecond decay of the out of plane vector, C_2 symmetry axis, and H—H intramolecular axis orientational correlation functions and found that, although the time scales differed, the non-Arrhenius behavior was the same (not shown). We find the activation energy is larger for the polarizable SPC/FQ model than the activation energy previously determined with the fixed-charge SPC/E model.[28] In that case the activation energies of 3.6 kcal/mol for both spectral diffusion and rotational relaxation were in good agreement with experiment. [28]

The similar temperature dependence for both these dynamics experiments (with activation energies of 3.4 kcal/mol for spectral diffusion and 3.7 kcal/mol for reorientation) suggests a common mechanism. Recent theoretical work by Laage and Hynes,[6,41] found that reorientation occurred through large amplitude angular jumps that exchanged a hydrogen bond with a small contribution from the diffusive motion of the hydrogen bond frame. This would suggest exactly what is observed in the current study since exchanging hydrogen bonds causes a significant change in frequency.[29] The authors also looked at the temperature dependence of reorientation and found that the large amplitude jumps and diffusive motion both contribute at every temperature but large amplitude jumps are dominant.[41]

In Figure 7 we show an Arrhenius plot that includes previous temperature-dependent studies of the first and second order orientational correlation functions along with the results of the current study. The barrier height is similar for all the experiments included in the figure, and a similar quadratic dependence is observed. The barrier heights from the plot range from 3.9 to 4.7 kcal/mol over liquid phase temperatures where 4.7 kcal/mol is from the dielectric relaxation (DR) study, which samples the higher slope portion of the curve. The ratio between $\tau_{R,2}$, measured in this study with pump-probe anisotropy, and $\tau_{R,1}$, measured with THz time domain spectroscopy (THz-TDS)[50] is 2.7 ± 0.1 over the temperature range in this study and there is no clear temperature dependence. We also plot the result of calculating $\tau_{R,2}$ derived from the Stokes-Einstein-Debye equation, $\tau_{R,2} = 4\pi\eta R^3/3kT$, where η is the temperature-dependent viscosity[56] and R is the hydrodynamic radius.[57] For both quantities we use the values for H_2O. The Stokes-Einstein-Debye (SED) equation assumes the reorientation is diffusive, which

predicts that the ratio between $C_{R,1}(t)$ and $C_{R,2}(t)$ is 3. We do not observe this ratio experimentally and reorientation dominated by diffusive steps disagrees with the theoretical work by Laage and Hynes.[6,41] However, the temperature dependence of τ_2 calculated with the SED equation shows a similar barrier height (4.3 kcal/mol) and quadratic behavior. Although we are comparing experiments that are each uniquely sensitive to the evolving structure of the liquid we observe a similar barrier and for the most part a similar quadratic behavior. This observation again points to the collective nature of the picosecond relaxation in water.

In previous studies, the non-Arrhenius behavior of thermodynamic and transport properties of water have been attributed to relaxation processes characteristic of supercooled liquids. Speedy and Angell found the temperature dependence of the isothermal compressibility, expansivity, isobaric heat capacity, diffusion coefficient, viscosity, dielectric relaxation, and ^{17}O spin relaxation rate followed power law behavior. A plot of relaxation rates against $\log\left(T/T_S - 1\right)$ using a homogeneous nucleation temperature T_S = 228 K was linear.[58,59] It has been suggested that water undergoes a fragile-to-strong transition at this temperature[60] and the relaxation processes subsequently assume an Arrhenius behavior until the glass formation temperature.[61] The Vogel-Fulcher-Tammann law, which has also been used to model relaxation rates in supercooled water, predicts a linear relationship between the log of the temperature dependence of the property and $1/\left(T - T_o\right)$.[52] Although several empirical relationships have been established, the microscopic explanation for the non-Arrhenius behavior in

terms of molecular behavior is unclear, and indicates a need for further studies at this level.

The common spectroscopic model ~~used~~ used in this study assumes the OD stretch is coupled to a thermally occupied harmonic bath, which makes predictions regarding the temperature dependence of spectral features.[34] The correlation function is proportional to the coupling parameter, λ, which is determined by fitting the FWHM of the linear absorption spectrum. At room temperature $\lambda = 2.7 \times 10^{-3}$ rad/fs, which represents a Stokes shift (2λ) of 29 cm^{-1}. If the input frequency and orientational correlation functions and lifetime are kept constant, and only the temperature is changed, the FWHM calculated with the model at the four other experimental temperatures are within ~1% of experimental values. However, the approximation predicts a linear relationship between temperature and FWHM and a quadratic relationship is observed experimentally (not shown). If the nonlinear measurements are calculated with the same input λ and correlation functions, and changing only ~~, frequency and orientational correlation functions, and lifetime, but with changing~~ temperature, there is a negligible difference in dynamics. Therefore, the correlation functions and spectral density of the bath is not temperature invariant, but are intrinsically different ~~must be adjusted~~ at each temperature ~~to match the experiment~~, which results in a different λ for each temperature (see Table 1).

The Stokes shift appears to make a small but non-negligible contribution to the spectroscopy (see, also, the supporting information). The value of 29 cm^{-1} is consistently smaller than prior determinations on the OH stretching vibration. ~~In 1999,~~ Woutersen and Bakker reported pump-probe experiments on the OH stretch of HOD in D_2O that probed relaxation dynamics ~~on the red and blue side of the line shape~~ upon pumping on the blue

and red side of the lineshape~~, respectively~~.[62] The authors used a Brownian oscillator model to fit the experimental traces and ~~report~~ extract a Stokes shift (2λ) of 74 cm^{-1}.[62] However, ~~with a response function formalism,~~ Yeremenko reproduced the results of Woutersen and Bakker without including a Stokes shift in the model, claiming that~~,~~ the observed behavior arises from the spectrally narrow pump and probe pulses interacting within the pulse duration.[45] For the same system, Dlott and co-workers found a Stokes shift of 120 ± 30 cm^{-1} by superimposing the Stokes Raman and anti-Stokes Raman peaks, which are sensitive to the ν=1←0 and ν=0←1 transitions, respectively.[63] With MD simulations, Lawrence and Skinner calculated a Stokes shift (2λ) of 57 cm^{-1} for the OH stretch of HOD in D_2O and 28 cm^{-1} for the OD stretch of HOD in H_2O, which is 1 cm^{-1} different from our experimental value.[19] ~~The Stokes shift appears to make a small but non-negligible contribution to the spectroscopy (see, also, the supporting information).~~

For isotopically dilute water, the vibrational relaxation of the OH stretch of HOD in D_2O has been more extensively studied both experimentally[25,64-66] and theoretically.[67-69] Nienhuys and Bakker[64,65] measured the temperature dependence of the vibrational lifetime and found it increased from 740 fs at 298 K to 900 fs at 363 K. Theoretical work by Rey and Hynes[69] and Lawrence and Skinner[67,68] found the overtone of the HOD bend was the dominant relaxation pathway, which agrees with the experimental temperature dependence. As the temperature is increased the stretch blue shifts and the bend red shifts toward their respective gas phase values. If the bend anharmonicity is constant with temperature the overtone will shift in the same manner as the bend and, therefore, the overlap integral between the overtone of the HOD bend and OH stretch will decrease resulting in a decrease in coupling and a longer lifetime. Dlott and co-workers have

performed the only experiments on isotopically dilute water that directly probe vibrations beyond the stretch after excitation of the stretch by using a mixed IR/Raman technique with ~1.5 ps time resolution.[66] They conclude that the primary route of energy relaxation of the OH stretch is through a pair of HOD bend vibrations facilitated by intermolecular energy transfer to D_2O. However, it is plausible that the overtone of the bend was not observed due to the experimental time resolution given that the lifetime of the fundamental of the HOD bend in D_2O is 390 fs.[70]

A theoretical study on the OD stretch of HOD in H_2O, performed similarly to the calculations on the OH stretch,[67-69] found the dominant pathway for the OD stretch was either through the fundamental of the HOD bend or directly to the ground state depending on if the bath was treated as rigid or flexible, respectively.[71] Fayer and co-workers originally measured a vibrational lifetime of the OD stretch of HOD in H_2O at room temperature of 1.45 ps[72] by using SVD analysis to account for the TSGS, then 1.7 ps[73] upon using a similar fitting method to Rezus and Bakker.[23] The longer lifetime of the OD stretch compared to the OH stretch agrees with the proposed mechanism for the OH stretch given that the closest intramolecular mode that is *lower* in energy, is separated by ~1050 cm^{-1}. Tielrooij and Bakker[43] measured the temperature-dependence and found it generally increased from approximately 1.7 to 2.2 ps from 274 to 343 K. In the current study we find the vibrational lifetime increases from 1.4 to 2.0 ps from 278 to 345 K (see Figure 3). These lifetimes are somewhat faster than those of Tielrooij[43] but agree with the lifetime first reported by Fayer and co-workers.[72] An important difference between the experiments is that the measurements in the former study are taken to $\tau_2 > 10$ ps but only to $\tau_2 \sim 4$ ps in the current study. An interesting similarity between the two

measurements, however, is that the vibrational lifetime of the OD stretch is largely unchanged from the lowest temperature to room temperature. Multiple competing pathways may exist that have different dependencies on temperature. The theoretical study, which was performed at room temperature, considered the rate constants for energy transfer to the fundamental of the HOD bend, and bend and stretch of H_2O;[71] but it did not consider a pathway through the overtone of the HOD bend, which is ~400 cm^{-1} higher in energy. Also, although the energy gap between the OD stretch and HOD bend increases with increasing temperature, the gap between the OD stretch and overtone decreases. The broad librational band of H_2O, which is peaked at ~680 cm^{-1},[74] or a combination of low frequency modes are capable of contributing the excess energy. An experimental study monitoring the deposition of energy into the HOD bend upon excitation of the OD stretch at multiple temperatures and a temperature-dependent theoretical study would helpful in determining if there is a change in mechanism with temperature.

VI. Conclusions

By using ultrafast infrared spectroscopy to measure the temperature-dependent picosecond decay of reorientation and spectral diffusion of the OD stretch of dilute HOD in H_2O, and comparing the non-Arrhenius behavior to previous measures of relaxation processes in water, we have found that hydrogen bond rearrangement in water is collective. To determine the picosecond decay we self-consistently model 2D IR, pump-probe, and linear absorption measurements with a response function formalism that includes the effects of spectral diffusion, population lifetime, reorientation, and non-

equilibrium heating upon vibrational relaxation. Prior experimental and theoretical studies have shown that hydrogen bond switching is concerted and involves large angle reorientation.[5,6] This work provides evidence that translation and reorientation are intertwined with hydrogen bond rearrangement in the collective reorganization of the liquid. It remains a question what the correlation length for reorganization is, which collective variables may be best suited to describe or study hydrogen bond rearrangement, and the microscopic origin of the non-Arrhenius behavior from the liquid to supercooled regions of water.

Acknowledgements

This work was supported by Basic Energy Sciences of the US Department of Energy under grant DE-FG02-99ER14988 to A.T. J.L.S. acknowledges support from NSF (CHE-0750307) and DOE (DE-FG02-09ER16110). R.A.N. and A.T. thank Sean Roberts, Krupa Ramasesha, and Kevin Jones for many helpful discussions. R.A.N. thanks the National Science Foundation for a Graduate Research Fellowship.

Supporting Information Available:

Dephasing functions for the response function formalism; Extracting the complex correlation, rephasing and non-rephasing 2D IR spectra from an absorptive 2D IR spectrum; Temperature-dependent parameters for the model for the OD stretch, H_2O stretch and combination band; Contribution of the H_2O stretch and combination band in the model; Contribution of reorientation and lifetime to the line shape; Effects of a

complex correlation function on the linear and 2D IR spectroscopy and the vibrational Stokes shift. This material is available free of charge via the Internet at http://pubs.acs.org.

Note: In a publication that was published during review, ~~Published while in review~~

~~In a recent publication,~~ Perakis and Hamm present 2D IR spectra of the OD stretch of HOD in H_2O from ambient temperature to the supercooled regime.[75] There are similarities with the current study: spectral diffusion slows with decreasing temperature and a slightly non-Arrhenius behavior is observed. However, the authors find a significant difference in barrier height depending on the polarization ~~geometry~~configuration used in the experiment. This is indicative of the ~~The~~ interesting and ~~possibly~~ complex relationship between OD frequency and OD reorientation, which ~~has just started to be explored~~[76,77] ~~and it~~ requires further experimental studies to be fully elucidated.

Formatted: TF_References_Section

References

1.Rahman, A.; Stillinger, F. H. Molecular dynamics study of liquid water. *J. Chem. Phys.* **1971**, *55*, 3336-3359.

2.Ohmine, I.; Tanaka, H. Fluctuations, relaxation, and hydration in liquid water: Hydrogen-bond rearrangement dynamics. *Chem. Rev.* **1993**, *93*, 2545-2566.

3.Stillinger, F. H.; Weber, T. A. Inherent structure in water. *J. Phys. Chem.* **1983**, *87*, 2833-2840.

4.Luzar, A.; Chandler, D. Effect of environment on hydrogen bond dynamics in liquid water. *Phys. Rev. Lett.* **1996**, *76*, 928-931.

5.Eaves, J. D.; Loparo, J. J.; Fecko, C. J.; Roberts, S. T.; Tokmakoff, A.; Geissler, P. L. Hydrogen bonds in liquid water are broken only fleetingly. *Proceedings of the National Academy of Sciences of the United States of America* **2005**, *102*, 13019-13022.

6.Laage, D.; Hynes, J. T. A molecular jump mechanism of water reorientation. *Science* **2006**, *311*, 833-835.

7.Skinner, J. L.; Bakker, H. J. Vibrational Spectroscopy as a Probe of Structure and Dynamics in Liquid Water. *Chemical Reviews* **2010**, *110*, 1498-1517.

8.Fecko, C. J.; Eaves, J. D.; Loparo, J. J.; Tokmakoff, A.; Geissler, P. L. Ultrafast Hydrogen-Bond Dynamics in the Infrared Spectroscopy of Water. *Science* **2003**, *301*, 1698-1698.

9.Rick, S. W.; Stuart, S. J.; Berne, B. J. Dynamical fluctuating charge force fields: Application to liquid water. *J. Chem. Phys.* **1994**, *101*, 6141-6156.

10.DeFlores, L. P.; Nicodemus, R. A.; Tokmakoff, A. Two-dimensional Fourier transform spectroscopy in the pump-probe geometry. *Optics Letters* **2007**, *32*, 2966-2968.

11.Gallagher Faeder, S. M.; Jonas, D. M. Two-dimensional electronic correlation and relaxation spectra: Theory and model calculations. *J. Phys. Chem. A* **1999**, *103*, 10489-10505.

12.Corcelli, S. A.; Skinner, J. L. Infrared and Raman line shapes of dilute HOD in liquid H_2O and D_2O from 10 to 90 ^oC. *J. Chem. Phys.* **2005**, *109*, 6154-6165.

13.Jorgensen, W. L.; Chandrasekhar, J.; Madura, J. D.; Impey, R. W.; Klein, M. L. Comparison of Simple Potential Functios for Simulating Liquid Water. *Journal of Chemical Physics* **1983**, *79*, 926-935.

14.Berendsen, H. J. C.; Grigera, J. R.; Straatsma, T. P. The Missing Term in Effective Pair Potentials. *J. Phys. Chem.* **1987**, *91*, 6269-6271.

15.Corcelli, S. A.; Lawrence, C. P.; Asbury, J. B.; Steinel, T.; Fayer, M. D.; Skinner, J. Spectral diffusion in a fluctuating charge model of water. *J. Chem. Phys.* **2004**, *121*, 8897-8900.

16.Adams, D. J.; Dubey, G. S. Taming the Ewald Sum in the Computer-Simulation of Charged Systems. *Journal of Computational Physics* **1987**, *72*, 156-176.

17.Auer, B.; Kumar, R.; Schmidt, J. R.; Skinner, J. L. Hydrogen bonding and Raman, IR, and 2D-IR spectroscopy of dilute HOD in liquid D_2O. *Proceedings of the National Academy of Sciences of the United States of America* **2007**, *104*, 14215-14220.

18.Janca, A.; Tereszchuk, K.; Bernath, P. F.; Zobov, N. F.; Shirin, S. V.; Polyansky, O. L.; Tennyson, J. Emission spectrum of hot HDO below 4000 cm(-1). *Journal of Molecular Spectroscopy* **2003**, *219*, 132-135.

19.Lawrence, C. P.; Skinner, J. L. Vibrational spectroscopy of HOD in liquid D_2O. II. Infrared line shapes and vibrational Stokes shift. *Journal of Chemical Physics* **2002**, *117*, 8847-8854.

20.Loparo, J. J.; Roberts, S. T.; Nicodemus, R. A.; Tokmakoff, A. Variation of the transition dipole moment across the OH stretching band of water. *Chemical Physics* **2007**, *341*, 218-229.

21.Schmidt, J. R.; Corcelli, S. A.; Skinner, J. L. Pronounced non-Condon effects in the ultrafast infrared spectroscopy of water. *J. Chem. Phys.* **2005**, *123*, 044513.

22.Loparo, J. J.; Roberts, S. T.; Tokmakoff, A. Multidimensonal infrared spectroscopy of water. I. Vibrational dynamics in 2D lineshapes. *Journal of Chemical Physics* **2006**, *125*, 194521.

23.Rezus, Y. L. A.; Bakker, H. J. On the orientational relaxation of HDO in liquid water. *Journal of Chemical Physics* **2005**, *123*, -.

24.Bakker, H. J.; Rezus, Y. L. A.; Timmer, R. L. A. Molecular reorientation of liquid water studies with femtosecond midinfrared spectroscopy. *Journal of Physical Chemistry A* **2008**, *112*, 11523-11534.

25.Loparo, J. J.; Fecko, C. J.; Eaves, J. D.; Roberts, S. T.; Tokmakoff, A. Reorientational and configurational fluctuations in water observed on molecular length scales. *Phys. Rev. B* **2004**, *70*, 180201.

26.Skinner, J. L.; Auer, B. M.; Lin, Y.-S. *Vibrational Lineshapes, Spectral Diffusion, and Hydrogen Bonding in Liquid Water*, 2009; Vol. 142.

27.Moilanen, D. E.; Fenn, E. E.; Lin, Y.-S.; J.L.Skinner; Bagchi, B.; Fayer, M. D. Water inertial reorientation: Hydrogen bond strength and the angular potential. *Proceedings of the National Academy of Sciences of the United States of America* **2008**, *105*, 5295-5300.

28.Nicodemus, R. A.; Ramasesha, K.; Roberts, S. T.; Tokmakoff, A. Hydrogen Bond Rearrangements in Water Probed with Temperature-Dependent 2D IR. *The Journal of Physical Chemistry Letters* **2010**, *1*, 1068-1072.

29.Loparo, J. J.; Roberts, S. T.; Tokmakoff, A. Multidimensonal infrared spectroscopy of water. II. Hydrogen bond switching dynamics. *Journal of Chemical Physics* **2006**, *125*, 194522.

30.Roberts, S. T.; Loparo, J. J.; Tokmakoff, A. Characterization of spectral diffusion from two-dimensional line shapes. *Journal of Chemical Physics* **2006**, *125*, 084502.

31.Asbury, J. B.; Steinel, T.; Kwak, K.; Corcelli, S. A.; Lawrence, C. P.; Skinner, J. L.; Fayer, M. D. Dynamics of water probed with vibrational echo correlation spectroscopy. *J. Chem. Phys.* **2004**, *121*, 12431-12446.

32.Demirdöven, N.; Khalil, M.; Tokmakoff, A. Correlated vibrational dynamics revealed by two-dimensional infrared spectroscopy. *Phys. Rev. Lett.* **2002**, *89*, 237401.

33.Kwak, K.; Park, S.; Finkelstein, I. J.; Fayer, M. D. Frequency-frequency correlation functions and apodization in two-dimensional infrared vibrational echo spectroscopy: A new approach. *Journal of Chemical Physics* **2007**, *127*, 124503.

34.Mukamel, S. *Principles of Nonlinear Optical Spectroscopy*; Oxford University Press: New York, 1995.

35.Fecko, C. J.; Loparo, J. J.; Roberts, S. T.; Tokmakoff, A. Local hydrogen bonding dynamics and collective reorganization in water: Ultrafast IR spectroscopy of HOD/D_2O. *J. Chem. Phys.* **2005**, *122*, 054506.

36.Saven, J. G.; Skinner, J. L. A molecular theory of the line shape: Inhomogeneous and homogeneous electronic spectra of dilute chromophores in nonpolar fluids. *Journal of Chemical Physics* **1993**, *99*, 4391-4402.

37.Lin, Y.-S.; Pieniazek, P. A.; Yang, M.; Skinner, J. L. On the calculation of rotational anistropy decay, as measured by polarization-resolved vibrational pump-probe experiments. *Journal of Chemical Physics* **2010**, *132*, 174505.

38.Schmidt, J. R.; Roberts, S. T.; Loparo, J. J.; Tokmakoff, A.; Fayer, M. D.; Skinner, J. L. Are water simulation models consistent with steady-state and ultrafast vibrational spectroscopy experiments? *Chemical Physics* **2007**, *341*, 143-157.

39.Lawrence, C. P.; Skinner, J. L. Quantum corrections in vibrational and electronic condensed phase spectroscopy: Line shapes and echoes. *Proceedings of the National Academy of Sciences of the United States of America* **2005**, *102*, 6720-6725.

40.Tokmakoff, A. Orientational correlation functions and polarization selectivity for nonlinear spectroscopy of isotropic media. I. Third order. *J. Chem. Phys.* **1996**, *105*, 1.

41.Laage, D.; Hynes, J. T. On the molecular mechanism of water reorientation. *Journal of Physical Chemistry B* **2008**, *112*, 14230-14242.

42.Stenger, J.; Madsen, D.; Hamm, P.; Nibbering, E. T. J.; Elsaesser, T. A photon echo peak shift study of liquid water. *J. Phys. Chem. A* **2002**, *106*, 2341-2350.

43.Tielrooij, K. J.; Petersen, C.; Rezus, Y. L. A.; Bakker, H. J. Reorientation of HDO in liquid H2O at different temperatures: Comparison of first and second order correlation functions. *Chemical Physics Letters* **2009**, *471*, 71-74.

44.Yeremenko, S.; Pshenichnikov, M. S.; Wiersma, D. A. Interference effects in IR photon echo spectroscopy of liquid water. *Phys. Rev. A* **2006**, *73*, 021804.

45.Yeremenko, S. Water dynamics explored by femotsecond infrared spectroscopy. Ph.D, University of Groningen, 2004.

46.Kozinski, M.; Garrett-Roe, S.; Hamm, P. 2D-IR spectroscopy of the sulfhydryl band of cysteines in the hydrophobic core of proteins. *Journal of Physical Chemistry B* **2008**, *112*, 7645-7650.

47.Chieffo, L.; Shattuck, J.; Amsden, J. J.; Erramilli, S.; Ziegler, L. D. Ultrafast vibrational relaxation of liquid H_2O following librational combination band excitation. *Chemical Physics* **2007**, *341*, 71-80.

48.Eaves, J. D.; Tokmakoff, A.; Geissler, P. L. Electric Field Fluctuations Drive Vibrational Dephasing in Water. *Journal of Physical Chemistry A* **2005**, *109*, 9424-9436.

49.Buchner, R.; Barthel, J.; Stauber, J. The dielectric relaxation of water between 0 C and 35 C. *Chem. Phys. Lett.* **1999**, *306*, 57.

50.Ronne, C.; Thrane, L.; Astrand, P. O.; Wallqvist, A.; Mikkelsen, K. V.; Keiding, S. R. Investigation of the temperature dependence of dielectric relaxation in liquid water by THz reflection spectroscopy and molecular dynamics simulation. *Journal of Chemical Physics* **1997**, *107*, 5319-5331.

51.Ludwig, R.; Weinhold, F.; Farrar, T. C. Experimental and Theoretical Determination of the Temperature-Dependence of Deuteron and Oxygen Quadrupole Coupling-Constants of Liquid Water. *Journal of Chemical Physics* **1995**, *103*, 6941-6950.

52.Lang, E. W.; Girlich, D.; Ludemann, H. D.; Piculell, L.; Muller, D. Proton Spin-Lattice Relaxation Rate in Supercooled H2O and H2O-(O-17) Under High Pressure. *Journal of Chemical Physics* **1990**, *93*, 4796-4803.

53.Winkler, K.; Lindner, J.; Bürsing, H.; Vöhringer, P. Ultrafast Raman-induced Kerr-effect of water: Single molecule versus collective motions. *J. Chem. Phys.* **2000**, *113*, 4674-4682.

54.Petersen, C.; Tielrooij, K. J.; Bakker, H. J. Strong temperature dependence of water reorientation in hydrophobic hydration shells. *Journal of Chemical Physics* **2009**, *130*, 214511-214511.

55.Ropp, J.; Lawrence, C. P.; Farrar, T. C.; Skinner, J. Rotational motion in liquid water is anisotropic: A nuclear magnetic resonance study. *J. Am. Chem. Soc.* **2001**, *123*, 8047-8052.

56.Cho, C. H.; Urquidi, J.; Singh, S.; Robinson, G. W. Thermal offset viscosities of liquid H2O, D2O, and T2O. *Journal Of Physical Chemistry B* **1999**, *103*, 1991-1994.

57.Eisenberg, D.; Kauzmann, W. *The Structure and Properties of Water*; Clarendon Press: Oxford, 1969.

58.Speedy, R. J.; Angell, C. A. Isothermal compressibility of supercooled water and evidence for a thermodynamic singularity at -45 C. *Journal of Chemical Physics* **1976**, *65*, 851-858.

59.Angell, C. A. *Water-A Comprehensive Treatise*; Plenum: New York, 1980; Vol. 7.

60.Ito, K.; Moynihan, C. T.; Angell, C. A. Thermodynamic determination of fragility in liquids and a fragile-to-strong liquid transition in water. *Nature* **1999**, *398*, 492-495.

61.Chen, S.-H.; Mallamace, F.; Mou, C.-Y.; Broccio, M.; Corsaro, C.; Faraone, A.; Liu, L. The violation of the Stokes-Einstein relation in supercooled water. *Proceedings of the National Academy of Sciences of the United States of America* **2006**, *103*, 12974-12978.

62.Woutersen, S.; Bakker, H. J. Hydrogen bond in liquid water as a brownian oscillator. *Phys. Rev. Lett.* **1999**, *83*, 2077-2081.

63.Deak, J. C.; Rhea, S. T.; Iwaki, L. K.; Dlott, D. D. Vibrational energy relaxation and spectral diffusion in water and deuterated water. *J. Phys. Chem. A* **2000**, *104*, 4866-4875.

64.Woutersen, S.; Emmerichs, U.; Nienhuys, H.-K.; Bakker, H. J. Anomalous temperature dependence of vibrational lifetimes in water and ice. *Phys. Rev. Lett.* **1998**, *81*, 1106-1109.

65.Nienhuys, H. K.; Woutersen, S.; Santen, R. A. v.; Bakker, H. J. Mechanism for vibrational relaxation in water investigated by femtosecond infrared spectroscopy. *J. Chem. Phys.* **1999**, *111*, 1494-1500.

66.Deàk, J. C.; Rhea, S. T.; Iwaki, L. K.; Dlott, D. D. Vibrational energy relaxation and spectral diffusion in water and deuterated water. *J. Phys. Chem. A* **2000**, *104*, 4866-4875.

67.Lawrence, C. P.; Skinner, J. L. Vibrational spectroscopy of HOD in liquid D_2O. I. Vibrational energy relaxation. *J. Chem. Phys.* **2002**, *117*, 5827-5838.

68.Lawrence, C. P.; Skinner, J. L. Vibrational spectroscopy of HOD in liquid D_2O. VI. Intramolecular and intermolecular vibrational energy flow. *J. Chem. Phys.* **2003**, *119*, 1623-1633.

69.Rey, R.; Hynes, J. T. Vibrational energy relaxation of HOD in liquid D2O. *J. Chem. Phys.* **1996**, *104*, 2356-2368.

70.Bodis, P.; Larsen, O. F. A.; Woutersen, S. Vibrational relaxation of the bending mode of HDO in liquid D2O. *Journal of Physical Chemistry A* **2005**, *109*, 5303-5306.

71.Tian, G. C. Molecular dynamics study on the vibrational energy relaxation of O-D stretch of HOD in liquid H2O. *Chemical Physics* **2006**, *328*, 216-220.

72.Steinel, T.; Asbury, J. B.; Zheng, J.; Fayer, M. D. Watching hydrogen bonds break: A transient absorption study. *Journal of Physical Chemistry A* **2004**, *108*, 10957-10964.

73.Piletic, I. R.; Moilanen, D. E.; Spry, D. B.; Levinger, N. E.; Fayer, M. D. Testing the core/shell model of nanoconfined water in reverse micelles using linear and nonlinear IR spectroscopy (vol 110, pg 4985, 2006). *Journal of Physical Chemistry A* **2006**, *110*, 10369-10369.

74.Max, J.-J.; Chapados, C. Isotope effects in liquid water by infrared spectroscopy. III. H2O and D2O spectra from 6000 to 0 cm-1. *Journal of Chemical Physics* **2009**, *131*, 184505.

75.Perakis, F.; Hamm, P. Two-Dimensional Infrared Spectroscopy of Supercooled Water. *J. Phys. Chem. B* **2010**.

76.Ramasesha, K.; Nicodemus, R. A.; Mandal, A.; Tokmakoff, A. Ultrafast Phenomena XVII, 2010, Snowmass, CO, USA.

77.Stirnemann, G.; Laage, D. Direct Evidence of Angular Jumps During Water Reorientation Through Two-Dimensional Infrared Spectroscopy. *J. Phys. Chem. Lett.* **2010**, *1*, 1511-1516.

Table 1: Summary of the temperature dependent parameters contained within our spectral model for the OD stretch of HOD in H_2O.

	278 K	286 K	295 K	323 K	345 K
ω_{10} [cm^{-1}] (from FTIR)	2499	2503	2508	2522	2534
ω_{10} [cm^{-1}] (input model)	2503	2507	2513	2529	2544
FWHM [cm^{-1}]	159	163	166	175	180
T_1 [ps]	1.4	1.5	1.4	1.6	2.0
$C_{R,2}(t)$ (A_R) τ_R [ps]	(0.74) 4.5	(0.64) 3.8	(0.69) 2.9	(0.78) 1.7	(0.78) 1.3
$C_\omega(t)$					
(A_1/λ) τ_1 [fs]	(0.41) 50	(0.44) 50	(0.45) 50	(0.57) 50	(0.71) 50
(A_1/λ) τ_2 [fs]	(0.35) 400	(0.33) 400	(0.35) 400	(0.27) 200	(0.12) 200
(A_1/λ) τ_3 [ps]	(0.24) 2.4	(0.23) 2.1	(0.2) 1.8	(0.16) 1.1	(0.17) 0.7
$\lambda/10^{-3}$ [rad/fs]	2.6468	2.5824	2.6993	3.1906	3.3834
$C_\omega'(0)/10^{-4}$ [rad^2/fs^2]	1.9467	1.9542	2.1062	2.7279	3.0922
$C_\omega''(0)/10^{-5}$ [rad^2/fs^2]	2.4284	2.5138	2.6956	4.1144	5.0896
Offset (PLS)	8.7e-2	8.0e-2	6.8e-2	1.1e-1	1.3e-1

Figure Captions

Figure 1: Temperature-dependent linear absorption of dilute HOD in H_2O with (a) and without (b) the solvent H_2O subtracted. The traces are offset along the absorbance axis. The fit from our spectral model is shown in dark gray for each temperature.

Figure 2: (a) Isotropic transient absorption (offset) and (b) anisotropy (normalized at 200 fs) of dilute HOD in H_2O at each of the five experimental temperatures plotted as a function of delay time between the pump and probe. The best fit from our spectral model normalized at 200 fs for both (a) and (b) is shown in dark gray. (c) Phase line slope over $\omega_1 = \omega_3 = 2470$ to 2530 cm^{-1} determined from the temperature and waiting time dependent 2D IR with the best fit from our model shown as solid lines.

Figure 3: Temperature-dependent lifetime, T_1, (open triangles), picosecond decay of the integrated pump-probe anisotropy (open squares) and picosecond decay of the best fit frequency correlation function from the fit model (open circles).

Figure 4: Experimental absorptive and phase 2D surfaces of dilute HOD in H_2O at each of the five temperatures at three waiting times: $\tau_2 = 160$ fs (top), 400 fs (middle) and 3.2 ps (bottom). The contours in the absorptive 2DIR spectra are at 12% intervals relative to the maximum. The phase spectra are plotted from $-\pi/2$ to $\pi/2$ and are windowed by 10% of the absolute value spectra.

Figure 5: First moment of the positive amplitude for slices in ω_1 at 2450 cm^{-1} (red) and 2550 cm^{-1} (blue) at the temperatures 295 K (a) and 278 K (b). The insets show the short time behavior for each of the two temperatures.

Figure 6: Absorptive and phase 2D surfaces calculated with the model at each of the five experimental temperatures at three waiting times: τ_2 = 160 fs (top), 400 fs (middle) and 3.2 ps (bottom). The contours in the absorptive 2DIR spectra are at 12% intervals relative to the maximum. The phase spectra are plotted from $-\pi/2$ to $\pi/2$ and are windowed by 10% of the absolute value spectra.

Figure 7: Arrhenius plot of the picosecond decay of the temperature-dependent best-fit frequency correlation function ($C_\omega(t)$, open circles) determined with the spectral model and anisotropy ($C_R(t)$, open squares) along with previous temperature-dependent measures of reorientational relaxation in water: optical Kerr effect[53] (OKE, filled circles), NMR[51] (crosses), terahertz time domain spectroscopy[50] (THz-TDS, asterisks), and dielectric relaxation[49] (DR, plusses). We also show the result of applying the Stokes-Einstein-Debye equation (SED, line).

Figure 8: Normalized temperature-dependent correlation functions for (a) the OD stretch vibrational frequency, $C_\omega(t)$, and (b) bond reorientation, $C_R(t)$, from MD simulations with the SPC/FQ water model. (c) Arrhenius plot of the correlation times in femtoseconds obtained from exponential fits to the picosecond decay.

Figure 1

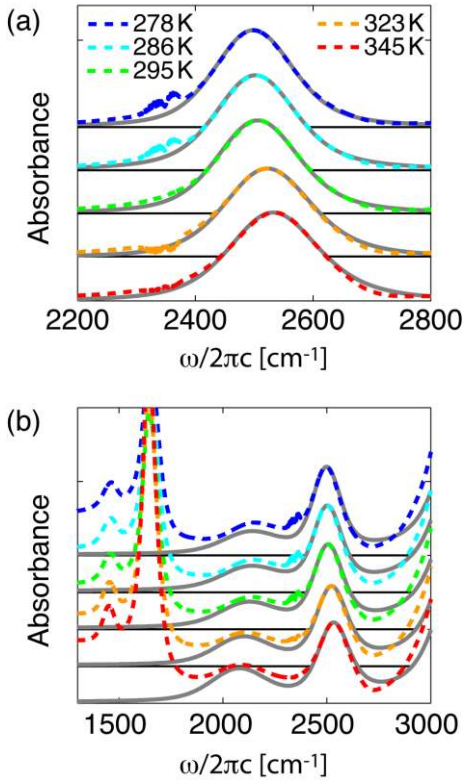
(a)
278 K
286 K
295 K
323 K
345 K
Absorbance
2200
2400
2600
2800
ω/2πc [cm-1]
(b)
Absorbance
1500
2000
2500
3000
ω/2πc [cm-1]

Figure 2

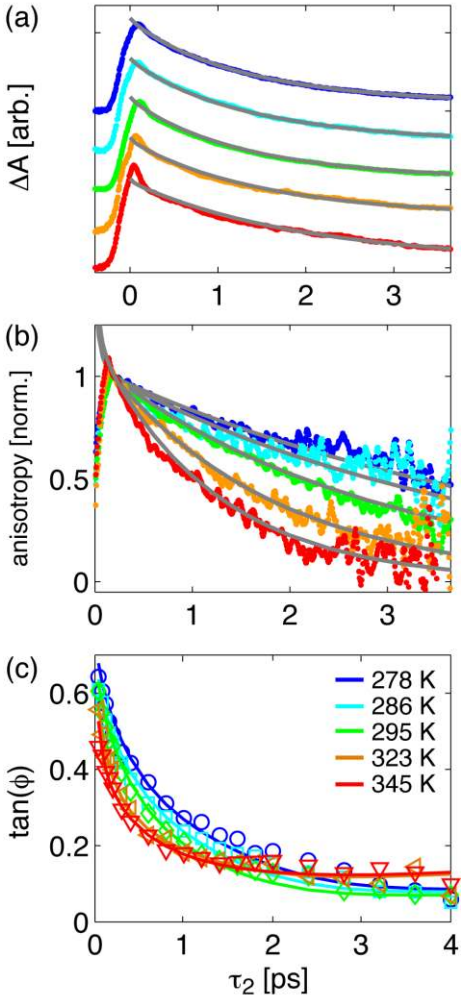
(a)
ΔA [arb.]
0
1
2
3
(b)
anisotropy [norm.]
1
0.5
0
0
1
2
3
(c)
tan(ϕ)
0.6
0.4
0.2
0
0
1
2
3
4
τ2 [ps]
278 K
286 K
295 K
323 K
345 K

Figure 3

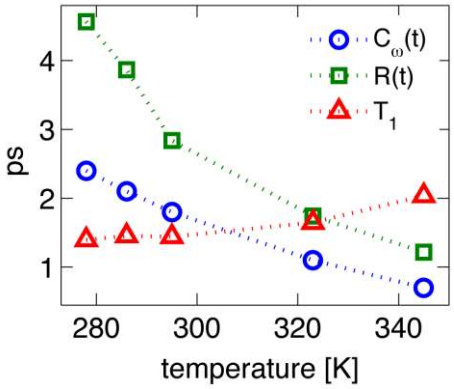

Figure 4

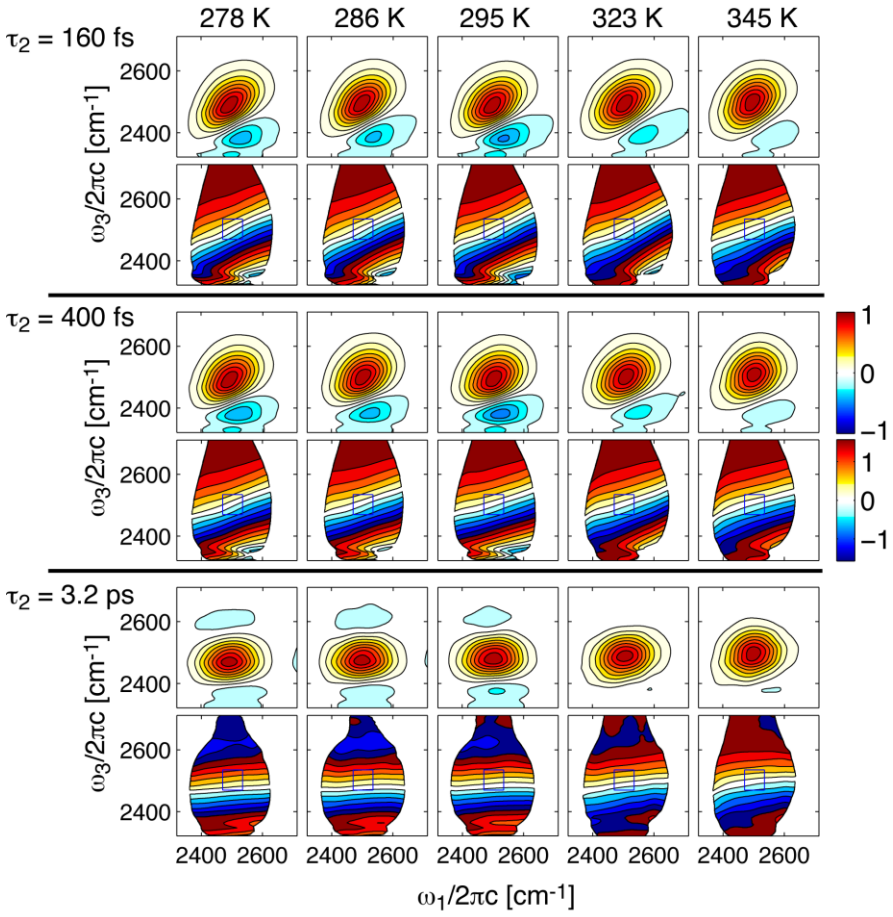
278 K
286 K
295 K
323 K
345 K
τ2 = 160 fs
τ2 = 400 fs
τ2 = 3.2 ps
ω3/2πc [cm-1]
2600
2400
1
0
−1
2400 2600
ω1/2πc [cm-1]

Figure 5

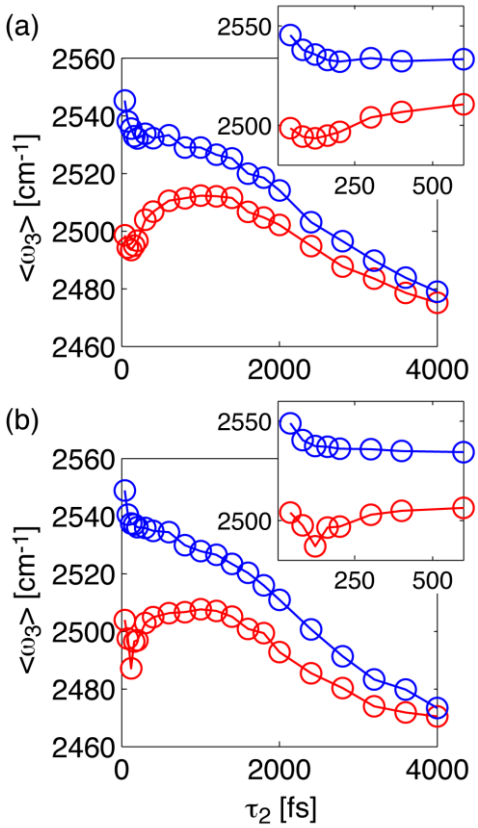
(a)
(b)
2560
2540
2520
2500
2480
2460
2550
2500
250
500
0
2000
4000
<ω3> [cm-1]
τ2 [fs]

Figure 6

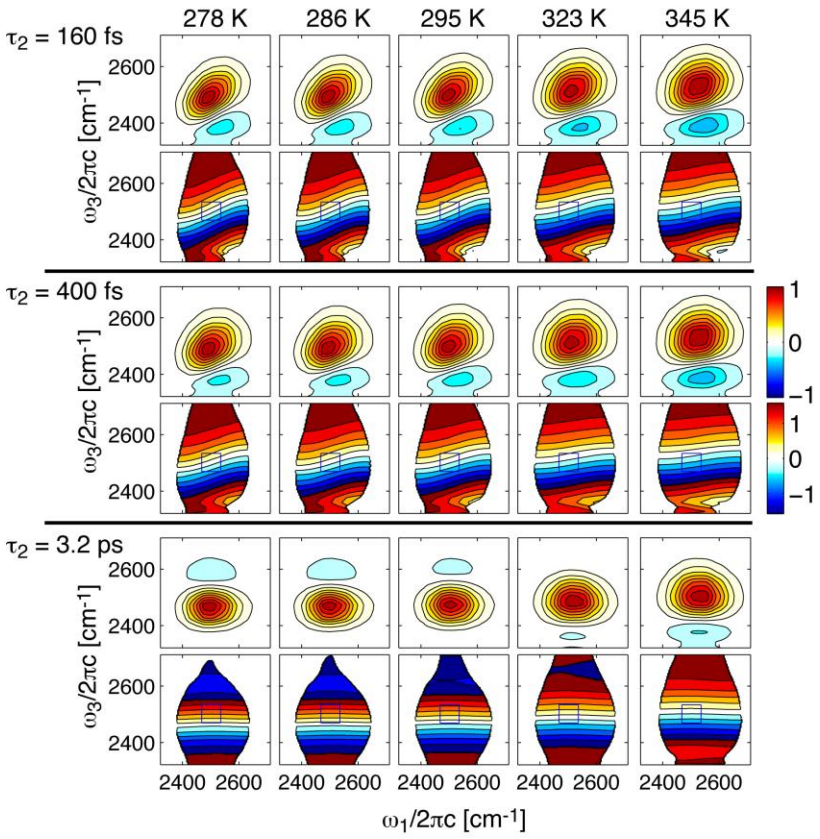
278 K
286 K
295 K
323 K
345 K
τ2 = 160 fs
τ2 = 400 fs
τ2 = 3.2 ps
ω3/2πc [cm-1]
2600
2400
1
0
−1
2400 2600
ω1/2πc [cm-1]

Figure 7

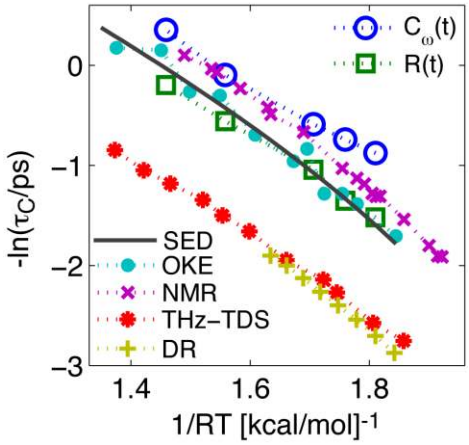
$C_\omega(t)$
R(t)
SED
OKE
NMR
THz–TDS
DR
$-\ln(\tau_C/ps)$
0
−1
−2
−3
1.4
1.6
1.8
1/RT [kcal/mol]$^{-1}$

Figure 8

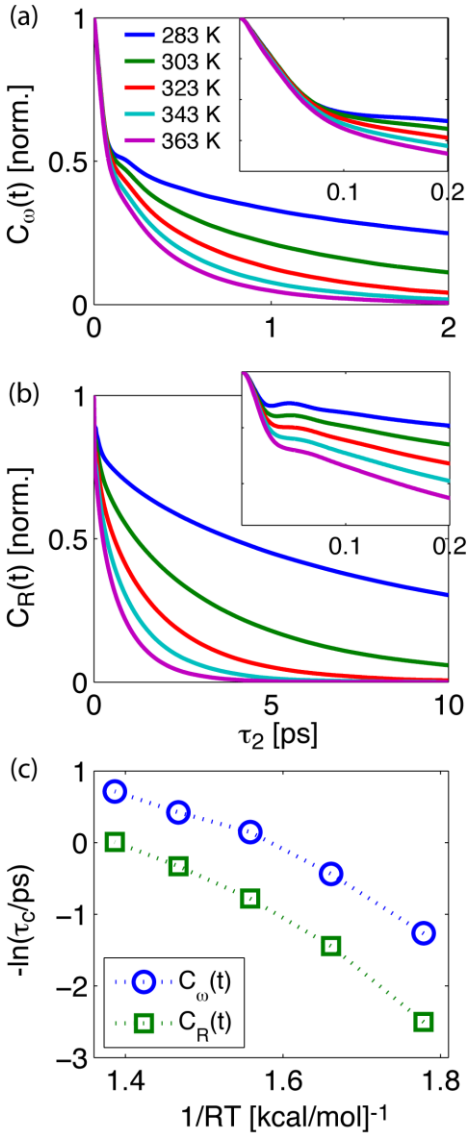
(a)
283 K
303 K
323 K
343 K
363 K
$C_\omega(t)$ [norm.]
(b)
$C_R(t)$ [norm.]
τ_2 [ps]
(c)
$-\ln(\tau_c/ps)$
$C_\omega(t)$
$C_R(t)$
1/RT [kcal/mol]$^{-1}$

Table of Contents (TOC) Figure